Magnetic, electric and electron magnetic resonance properties of orthorhombic self-doped $La_{1-x}MnO_3$ single crystals

2003 J. Phys.: Condens. Matter 15 3985

(http://iopscience.iop.org/0953-8984/15/23/311)

INSTITUTE OF PHYSICS PUBLISHING JOURNAL OF PHYSICS: CONDENSED MATTER

J. Phys.: Condens. Matter **15** (2003) 3985–4000 PII: S0953-8984(03)62512-9

Magnetic, electric and electron magnetic resonance properties of orthorhombic self-doped $La_{1-x}MnO_3$ single crystals

V Markovich[1,6], I Fita[2,3], A I Shames[1], R Puzniak[2], E Rozenberg[1], Ya Yuzhelevski[1], D Mogilyansky[4], A Wisniewski[2], Ya M Mukovskii[5] and G Gorodetsky[1]

[1] Department of Physics, Ben-Gurion University of the Negev, 84105, Beer-Sheva, Israel
[2] Institute of Physics, Polish Academy of Sciences, Aleja Lotnikow 32/46, PL-02-668 Warsaw, Poland
[3] Donetsk Institute for Physics and Technology, National Academy of Sciences, R Luxemburg Street 72, 83114, Donetsk, Ukraine
[4] Institute of Applied Research, Ben-Gurion University of the Negev, 84105, Beer-Sheva, Israel
[5] Moscow State Steel and Alloys Institute, 117936, Moscow, Russia

E-mail: markoviv@bgumail.bgu.ac.il

Received 24 April 2003
Published 30 May 2003
Online at stacks.iop.org/JPhysCM/15/3985

Abstract

The effect of lanthanum deficiency on structural, magnetic, transport, and electron magnetic resonance (EMR) properties has been studied in a series of $La_{1-x}MnO_3$ ($x = 0.01, 0.05, 0.11, 0.13$) single crystals. The x-ray diffraction study results for the crystals were found to be compatible with a single phase of orthorhombic symmetry. The magnetization curves exhibit weak ferromagnetism for all samples below 138 K. It was found that both the spontaneous magnetization and the coercive field increase linearly with x. The pressure coefficient dT_N/dP decreases linearly with self-doping, from a value of 0.68 K kbar^{-1} for $La_{0.99}MnO_3$ to 0.33 K kbar^{-1} for $La_{0.87}MnO_3$. The resistivity of low-doped $La_{0.99}MnO_3$ crystal is of semiconducting character, while that of $La_{0.87}MnO_3$ depends weakly on temperature between 180 and 210 K. It was found that the magnetic and transport properties of the self-doped compounds may be attributed to a phase separation involving an antiferromagnetic matrix and ferromagnetic clusters. The latter phases as well as their paramagnetic precursors have been directly observed by means of EMR.

1. Introduction

The stoichiometric lanthanum manganite $LaMnO_3$ is an A-type antiferromagnetic (AFM) insulator having a Néel temperature $T_N \approx 140$ K [1, 2]. Its weak ferromagnetic (FM) moment may arise due to a Dzyaloshinskii–Moriya (DM) interaction [2]. At room temperature

[6] Author to whom any correspondence should be addressed.

this compound has an orthorhombic perovskite structure with space group *Pnma* and antiferrodistortive orbital ordering (OO) of the Mn–O bond configuration. Alternating long and short Mn–O distances in the *ac*-plane are a hallmark of OO, which results from cooperative Jahn–Teller (JT) distortions [3]. Doping of the parent $LaMnO_3$ with divalent ions (A = Ca, Sr, Ba, etc) on La sites results in the appearance of a plethora of magnetic and crystallographic structures manifesting themselves in the rich phase diagrams of doped La manganites, $La_{1-x}A_xMnO_3$—see [1]. It is widely accepted nowadays [1] that the current carriers in $La_{1-x}A_xMnO_3$, at least at moderate x, are mobile holes, which appear due to charge compensation and move from Mn^{4+} ions to normal-valence Mn^{3+} ions. These holes simultaneously dominate the transport and mediate the FM double-exchange (DE) interaction. On the other hand, the superexchange (SE) interactions may cause FM or AFM insulating phases. The important role of the JT effect in the conductivity of doped manganites was pointed out in [4].

In addition to the above-noted doping with divalent ions, the effect of so-called 'self-doping' is also observed for $LaMnO_3$. It demonstrates a wide range of off-stoichiometric oxidation on the La sites and Mn sites. Although the common formula used for the off-stoichiometric compound is $LaMnO_{3+\delta}$, the perovskite structure cannot accommodate the excess of oxygen in interstitial sites and the oxygen excess accounts for the cationic vacancies [5]. In this case the chemical formula should be rewritten in the form $La_{1-x}Mn_{1-y}O_3$. The evolution of the crystal structure and magnetic order with progressive self-doping for the above $La_{1-x}Mn_{1-y}O_3$ compounds was investigated in [6–12]. At room temperature the orthorhombic O′ phase ($c/\sqrt{2} < a < b$) persists over the range $0 \leqslant \delta \leqslant 0.06$, whereas the rhombohedral phase is stable for $0.1 \leqslant \delta \leqslant 0.18$ [6]. As pointed out by Topfer and Goodenough [6], orthorhombic samples with small contents of cation vacancies may contain superparamagnetic clusters distributed in the AFM matrix and exhibit a spin-glass behaviour below T_N. Alternatively, Prado *et al* [7] proposed that the magnetization of the orthorhombic phase with cation vacancies results mostly from the increase in the canting of the spin arrangement. The magnetic and transport properties of $La_{1-x}MnO_{3-\delta}$ ($0.67 < 1-x < 1$) epitaxial thin films were analysed by Gupta *et al* [12]. The above films exhibit a FM transition at temperatures ranging from 115 to 240 K, and the transition temperature increases with progressive La deficiency. It is important to note here that, according to data from [11], the limiting value of x which may be accommodated in La sites of $La_{1-x}MnO_3$ compounds is only 0.125.

In general, transport and magnetic properties of doped La manganites are quite sensitive to magnetic and electric fields, pressure, light, and x-rays [1]. At the same time, the effect of external perturbations on the physical properties of self-doped $La_{1-x}Mn_{1-y}O_3$ and the parent undoped $LaMnO_3$ compounds has been considerably less fully investigated. The following important results may be noted. The effects of applied pressure (P) on the transport properties of self-doped $La_{0.91}Mn_{0.95}O_3$ ceramics [13] and $La_{0.94}Mn_{0.98}O_3$ crystal [14], with predominant ferromagnetic metallic (FMM) and ferromagnetic insulating (FMI) ground states, respectively, resemble the transport behaviour of hole-doped manganites. Measurements on $LaMnO_3$ under high P were performed recently [15–17]. Neutron diffraction [15] and combined Raman and x-ray data [16] for $LaMnO_3$ show that applied pressure decreases the orthorhombic distortions. The Néel temperature of $LaMnO_3$ exhibits under pressure an intricate behaviour. According to neutron diffraction data [15], $dT_N/dP = 0.32$ K kbar^{-1}, whereas ac susceptibility measurements show a non-linear behaviour of this parameter below 7 kbar and a higher value of about 0.55 K kbar^{-1} at $P > 7$ kbar [17].

To the best of our knowledge no investigations have been carried out on the effect of current on transport properties of self-doped manganites. On the other hand, it is observed that

electric field/current causes destabilization of the charge ordering [18] and induces metastable resistivity [19] in doped manganites. Electron magnetic resonance (EMR), comprising electron paramagnetic resonance (EPR) and ferromagnetic resonance (FMR), is known to be highly sensitive to minute magnetic phases. This allows direct observation of such phases even for self-doped manganites with very small off-stoichiometry.

In this paper we report on measurements of the magnetization (under ambient and high hydrostatic pressure), resistivity (changes of conductivity under external magnetic and electric fields), and EMR carried out on the series of self-doped single crystals $La_{1-x}MnO_3$ ($x = 0.01$–0.13). Systematical studies of variation of the above physical properties with increasing x and their comparison with the properties of 'usual' doped manganites are important for achieving progress in our understanding of the nature of the magnetic ordering and conductivity in self-doped La manganites.

2. Experiment

Single crystals of $La_{1-x}MnO_3$ ($x = 0.01$, 0.05, 0.11, 0.13) were grown by a floating zone method using radiative heating [20]. The chemical composition of the above samples was examined by inductively coupled plasma atomic emission spectroscopy. The results obtained were found to be in agreement with the nominal compositions of the starting materials. Samples of $7 \times 3 \times 2$ mm^3 having their longest dimension along the $\langle 110 \rangle$ direction, were cut out of the bulk crystal and used for electrical resistance measurements. Cylinder-shaped samples having a diameter of 1 mm and height of 3.5 mm with a $\langle 110 \rangle$ axis of rotation were used for the measurements of magnetization under hydrostatic pressure.

Preliminary evaporated silver strips with a separation of about 0.5 mm between the voltage (V) contacts were used for the customary four-point resistance measurements. The resistivity for various temperatures (T) and magnetic fields was measured while a dc current of 50 μA was flowing through the sample. Measurements of the magnetoresistance (MR) were carried out at magnetic fields H up to 15 kOe, aligned parallel to the current direction. AC measurements of the differential resistance ($R_d = \mathrm{d}V/\mathrm{d}I$) were performed using a lock-in technique and a modulation current 5 μA at 390 Hz. For the measurements of R_d versus bias current the applied current I was limited to prevent heating of the samples. Magnetic measurements under pressure were performed in the temperature range 4.2–220 K and in H up to 15 kOe using a PAR (Model 4500) vibrating sample magnetometer. Details of such measurements under pressure are reported elsewhere [21].

The EMR measurements on polycrystalline loose-packed samples were carried out at $120\ \mathrm{K} \leqslant T \leqslant 500\ \mathrm{K}$ using a Bruker EMX-220 digital X-band ($\nu = 9.4$ GHz) spectrometer. Small pieces of $La_{0.99}MnO_3$ and $La_{0.87}MnO_3$ crystals were crushed to fine powder and then put into the glass capillary tubes and centred in the rectangular cavity. EMR spectra were recorded at 200 μW incident microwave power and 100 kHz magnetic field modulation of 10 Oe amplitude. The spectra processing was performed using Bruker WIN-EPR Software and the values of the resonance fields (g-factors) were determined from the second derivative of the EMR absorption spectra.

3. Results

3.1. X-ray diffraction

The structure and phase purity of the samples were checked by means of x-ray powder diffraction at room temperature. The x-ray data were found to be compatible with the orthorhombic

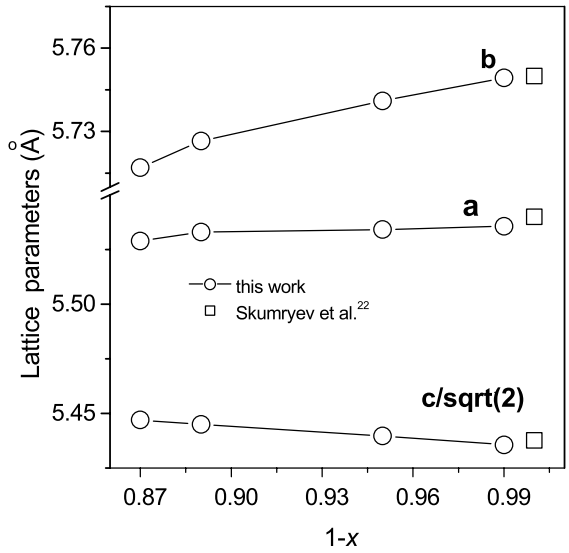

Figure 1. The lattice parameters of the orthorhombic unit cell of $La_{1-x}MnO_3$ single crystals for various doping levels.

unit cell (*Pnma* symmetry). Figure 1 shows the cell parameters for various La contents. For comparison, the lattice parameters of the unit cell for $LaMnO_3$ crystal [22] are also shown in figure 1. It should be noted that at room temperature all samples fulfil the criterion $c/a < \sqrt{2}$, typical for cooperative JT deformation superimposed on the orthorhombic structure [7]. Maurin *et al* [23] have found that the volume of the unit cell varies linearly with the Mn^{4+} content up to 30% of Mn^{4+}, which corresponds to a limit of solubility for La and Mn vacancies. The expression relating the unit-cell volume U per formula unit to the Mn^{4+} content is given by Maurin *et al* [23]:

$$y = (61.03 - U\ (\text{Å}^3))/0.096, \tag{1}$$

where y is the percentage of Mn^{4+}.

According to equation (1) and the unit-cell volume determined, the total variation of Mn^{4+} in our samples does not exceed 3%. Equation (1) is an empirical expression from experimental results on $LaMnO_{3+\delta}$ and $La_{1-x}Ca_xMnO_3$ ceramic samples [23]. It is supposed in the following discussion that the above relation (equation (1)) holds also for self-doped samples of orthorhombic structure and low deficiency of cations.

3.2. Magnetic measurements

Figure 2 presents field-cooled (FC) and zero-field-cooled (ZFC) magnetization curves, for $La_{0.99}MnO_3$ crystal, for H aligned in the (110) plane. The magnetization curves obtained for other crystals are similar to those shown in figure 2. It should be noted that the FC magnetization M_{FC} at low temperatures increases with the self-doping, whereas the ZFC magnetization, M_{ZFC} is practically unchanged. Moreover, with increasing T, M_{ZFC} exhibits a sharp increase at $T \approx 133$ K and then approaches zero. In the present work, the abrupt change in the magnetization M_{FC} during cooling is identified as the magnetic transition temperature T_N.

The hysteresis loop at $T = 5$ K for $La_{0.99}MnO_3$ crystal is given in figure 3(a). It exhibits a weak FM moment, which may result from a DM interaction as well as from FM clusters.

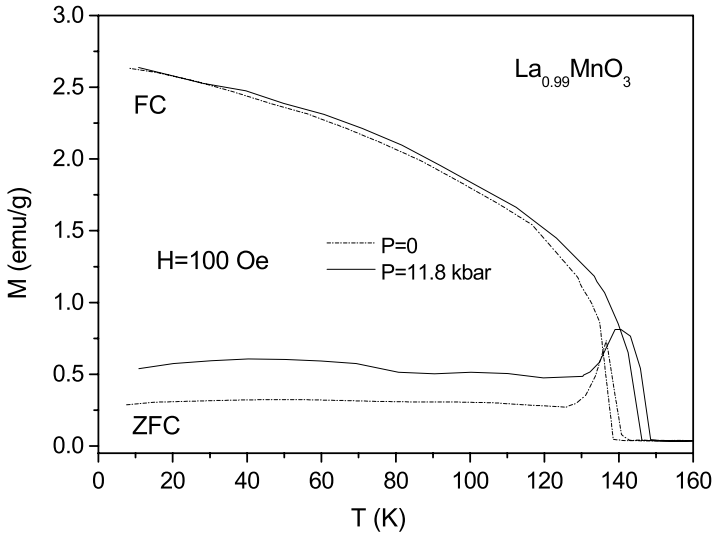

Figure 2. The FC (M_{FC}) and ZFC magnetization (M_{ZFC}) of $La_{0.99}MnO_3$ crystal, measured at an applied magnetic field $H = 100$ Oe for $P = 0$ and 11.8 kbar.

The spontaneous magnetization M_0 was obtained by linear extrapolation of the high-field magnetization to $H = 0$. Figures 3(b), (c) present the variations of the coercive field H_C and M_0 with the level of self-doping. For comparison, the spontaneous magnetization of $La_{0.9}MnO_3$ crystal [10] is also given in figure 3(b). Measurements of the magnetization at various temperatures and magnetic fields—see, for example, figures 2 and 3(a)—were carried out along the direction exhibiting the maximal value of magnetization in the (110) plane. This direction was determined by rotating of samples around the ⟨110⟩ axis in $H = 10$ kOe.

The following features characterize the magnetization of the self-doped samples under pressure:

(i) T_N increases with pressure—see figure 2;
(ii) the values of M_{FC} for each sample at low temperatures practically coincide for all P;
(iii) the hysteresis loops at $T = 5$ K are almost independent of pressure.

Though the Néel temperature depends only slightly on the level of self-doping, its pressure coefficient, dT_N/dP, depends strongly in an almost linear manner on x; see figure 4. Such a coefficient, dT_N/dP, for the parent $LaMnO_3$ [17] is added for comparison in figure 4(b), and this agrees fairly well with the linear dependence obtained for our samples.

3.3. Transport properties

Figure 5 shows the temperature dependence of the resistivity $\rho(T)$ observed for the $La_{1-x}MnO_3$ ($x = 0.01$, 0.11, 0.13) crystals at current $I = 50$ μA, upon cooling. For the $La_{0.99}MnO_3$ crystal, the $\rho(T)$ curve obeys well the exponential dependence $\rho(T) = \rho_0 \exp(E_a/kT)$ with activation energy $E_a = 0.20$ eV over a wide temperature range, $190 \leqslant T < 300$ K (see figure 5). The resistivities of $La_{0.89}MnO_3$ and $La_{0.87}MnO_3$ also obey the above expression for $\rho(T)$ but in narrower temperature ranges. For $La_{0.89}MnO_3$ and $La_{0.87}MnO_3$ we found $E_a = 0.19$ eV at temperatures $225 < T < 300$ K and $E_a = 0.18$ eV for $250 < T < 300$ K, respectively. For the parent $LaMnO_3$, the activation energy obtained is $E_a = 0.26$ eV [24]. In

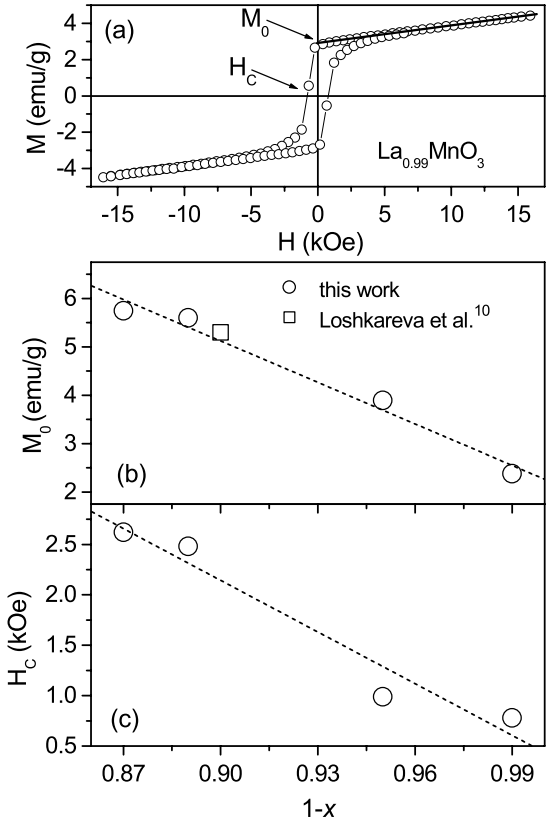

Figure 3. The hysteresis loop of $La_{0.99}MnO_3$ crystal (a) taken at $T = 5$ K; the spontaneous magnetization (b) and coercive field (c) of $La_{1-x}MnO_3$ single crystals at $T = 5$ K for various levels of self-doping.

the case of $La_{0.87}MnO_3$, the ρ versus T dependence is very weak between 180 and 210 K—see figure 5. A similar reduction of E_a with progressive La deficiency was observed earlier in $La_{1-x}MnO_{3-\delta}$ ($0.67 < 1-x < 1$) epitaxial thin films, reflecting the enhancement of the Mn^{4+} content [12].

Measurements of the resistivity $\rho(T)$ in various external fields H or for various bias currents I were performed as a part of the transport studies. The effect of magnetic field up to 15 kOe on the resistivity of $La_{0.99}MnO_3$ crystal is practically invisible in the temperature range $180 < T < 295$ K. At room temperature the bias current has no effect on the resistivity of this crystal, while at 200 K a definite increase of ρ with current is observed. A significant difference between the effects of magnetic field and bias current on the resistivities of $La_{0.87}MnO_3$ crystal and those on the $La_{0.99}MnO_3$ sample can be seen in figure 6. Figure 6(a) shows MR versus H at various temperatures. One should note that at room temperature a very small MR effect is observed. 'Usual' optimally doped manganites exhibit colossal MR near their Curie temperature [1]. In contrast, the negative MR effect observed for the $La_{0.87}MnO_3$ sample is strongest at $T = 200\ \text{K} > T_N$—see figure 6(a). Figure 6(b) shows the normalized differential resistivity $R_d(I)/R_d(0)$ of $La_{0.87}MnO_3$ as a function of current flow at various values of T. Only a small influence of the current on R_d is observed even at room temperature, whereas below 220 K the effect of the electrical current on R_d increases with decreasing T.

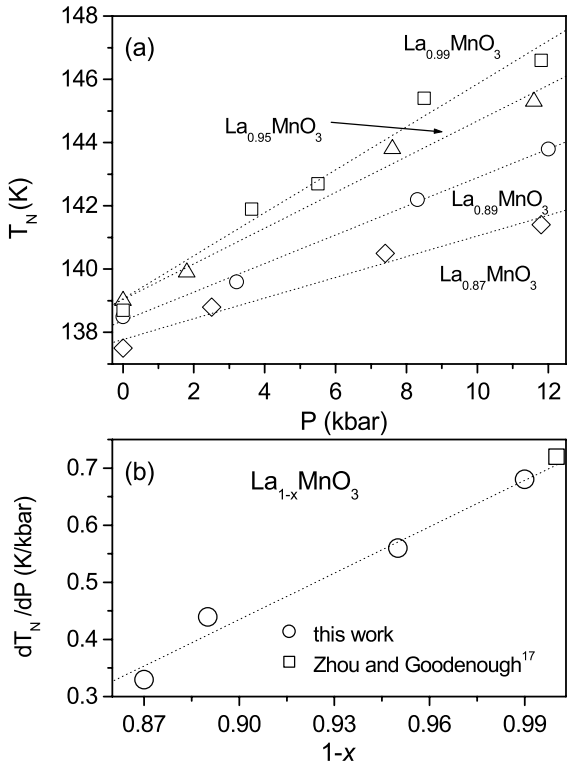

Figure 4. (a) The pressure dependence of the magnetic transition temperature of $La_{1-x}MnO_3$ single crystals. The dotted lines show the linear fitting. (b) The pressure coefficient as a function of the self-doping.

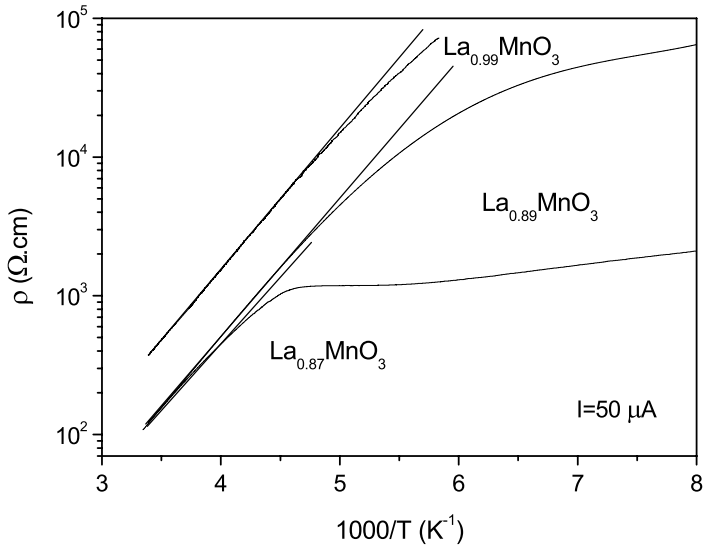

Figure 5. The resistivity ρ of $La_{1-x}MnO_3$ single crystals as a function of temperature. The straight lines are fits of initial slopes (see the text).

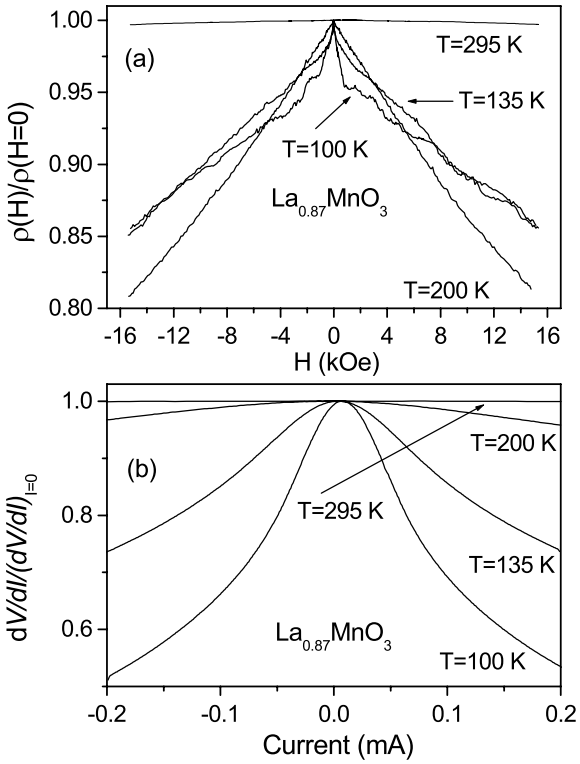

Figure 6. The magnetic field dependence of the normalized resistivity of $La_{0.87}MnO_3$ single crystal at various temperatures (a) and the normalized differential resistivity $(dV/dI)/(dV/dI)_{I=0}$ of $La_{0.87}MnO_3$ crystal versus the current at various temperatures (b).

3.4. Electron magnetic resonance

Temperature dependences of the EMR spectra for $La_{0.99}MnO_3$ and $La_{0.87}MnO_3$ samples are shown in figures 7(a) and 8, respectively. For each sample two types of EMR signals were observed:

(1) broad asymmetric lines shifted from $g = 2.0$ position at temperatures below some $T = T_p$;
(2) a superposition of two overlapping signals above T_p.

Figure 7(b) shows a decomposition of the experimental spectrum of the $La_{0.99}MnO_3$ sample at $T = 180$ K ($T > T_p$), into two symmetric lines—broad and narrow. The low-temperature signals obtained are typical for FM ordered phases observed in doped manganites (see [21] and references therein). The symmetric lines, observed at higher temperatures ($T \geqslant 180$ K, $La_{0.99}MnO_3$ and $T \geqslant 235$ K, $La_{0.87}MnO_3$), are attributed to the paramagnetic (PM) precursors of the aforementioned FM phases.

For both $La_{0.99}MnO_3$ and $La_{0.87}MnO_3$ samples the double-integrated intensities (DIN) of the EMR spectra increase continuously with lowering temperature, reaching a maximum at $T = T_{max}$ and then dropping upon further decrease of T; see figure 9. However, these samples differ in the content of the magnetically ordered component—see figure 9, which shows the DIN values (proportional to microwave magnetic susceptibility) for the two samples, normalized to their high-temperature PM values at $T = 480$ K.

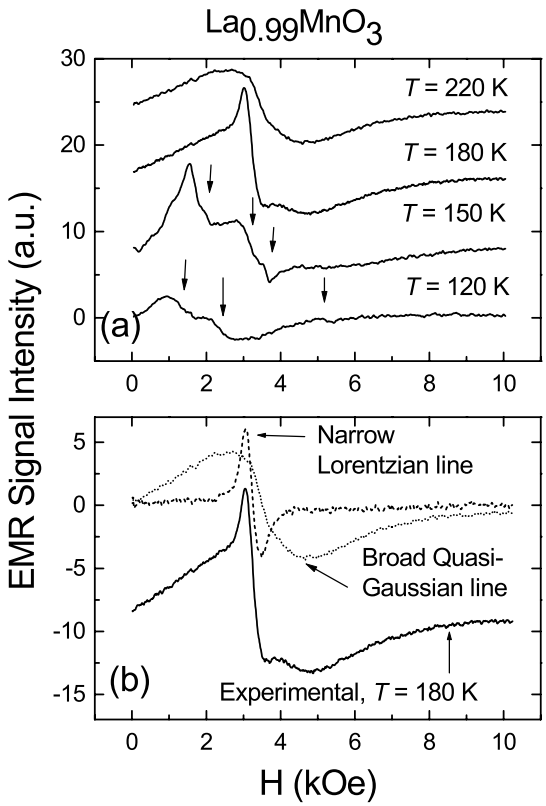

Figure 7. The temperature dependence of EMR spectra for $La_{0.99}MnO_3$, $\nu = 9.43$ GHz: (a) arrows point to three FMR signals; (b) decomposition of the EMR spectrum at $T = 180$ K into two symmetric lines: narrow Lorentzian and broad quasi-Gaussian ones.

The upper spectrum of $La_{0.99}MnO_3$ shown in figure 7(a) displays, as already noted before, a typical EMR signal at 220 K $\leqslant T \leqslant$ 500 K, which consists of a broad singlet line ($\Delta H_{pp} \sim 2200$ kOe at 300 K) of quasi-Gaussian shape, centred at $g = 1.91 \pm 0.05$—see figure 10(a). When T decreases below 220 K, an additional weak and narrower resonance line with $g = 1.97 \pm 0.01$ may be revealed by using the second derivative of the EMR absorption spectra. The latter line becomes more distinguishable below 200 K (see figure 7(a)). This line has a symmetric Lorentzian-like shape (see the decomposition in figure 7(b)); its ΔH_{pp} passes through a minimum at $T_{min} = 190$ K and then broadens again (figure 11(a)). At $T = 190$ K, both lines are well observed, although the intensity of the narrow line does not exceed 10% of the total DIN, as presented in figure 9. Below $T_{p1} = 175$ K the symmetric line turns into three asymmetric lines. These lines overlap with the quasi-Gaussian broad line which abruptly disappears when the temperature drops below $T_{p2} = 140$ K. When the temperature decreases to $T = 120$ K, two of those asymmetric lines shift towards low fields and the other one shifts towards high fields—see figure 7(a) (line positions indicated by arrows).

Figure 8 represents changes in the EMR spectra of $La_{0.87}MnO_3$ within the same temperature region of 120 K $\leqslant T \leqslant$ 500 K. Like in the case of $La_{0.99}MnO_3$, the EMR spectra in the PM region ($T \geqslant 235$ K) consist of two overlapping resonance lines: a broad one and a narrow Lorentzian-like line—see figure 8(a). The broad line is observed down to 240 K. At lower temperatures other broad resonance lines, originating from magnetically ordered phases, appear. The overlap of the lines throughout the whole PM region prevented

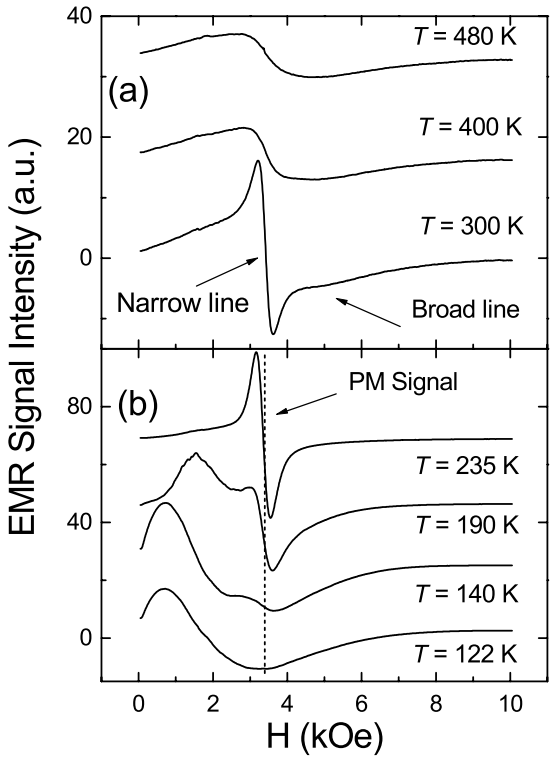

Figure 8. The temperature dependence of the EMR spectra for $La_{0.87}MnO_3$, $\nu = 9.43$ GHz: (a) the PM region; (b) the FM region: the vertical line indicates the position of the high-temperature PM signal.

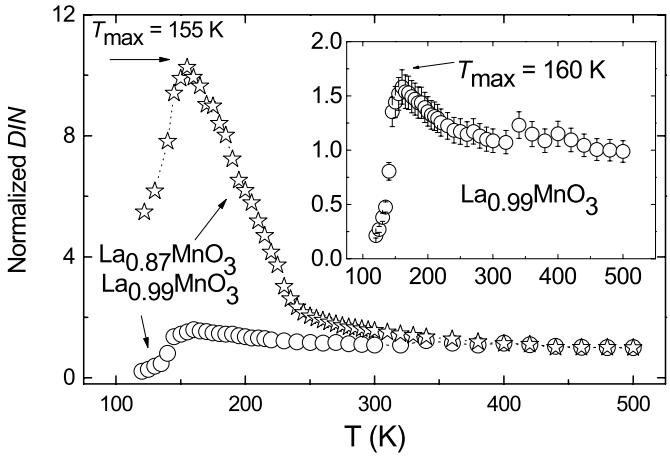

Figure 9. The temperature dependence of DIN of the EMR spectra, normalized to the DIN value at $T = 480$ K: circles—$La_{0.99}MnO_3$; stars—$La_{0.87}MnO_3$. Inset—a zoom of the $La_{0.99}MnO_3$ temperature dependence. Lines are guides for the eyes.

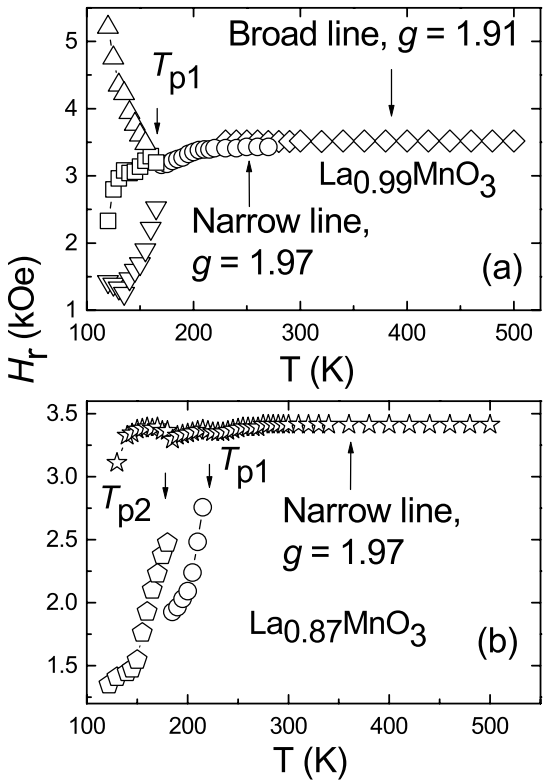

Figure 10. Temperature dependences of the resonance fields: (a) $La_{0.99}MnO_3$: diamonds—broad PM line; circles—narrow PM line; triangles pointing up and down—two components of the FMI signal; squares—FMM signal; (b) $La_{0.87}MnO_3$: stars—narrow PM line; circles—one FMM phase; pentagons—another FMM phase. Lines are guides for the eyes.

a precise determination of the g-value for that broad line. It may just be estimated that, like in the case of $La_{0.99}MnO_3$, the g_{broad}-value is lower then the g_{narrow}-value. The same signal overlapping prevents measurements of the width of the broad line. The narrow Lorentzian-like line was observed in all EMR spectra above 125 K. It is compatible with $g = 1.97$ at the high-temperature limit and slightly shifts toward low field when approaching temperatures designated as T_p (figure 10(b)). On decreasing temperature, the width of the narrow line decreases, passes through a minimum at $T_{min1} = 260$ K, and then starts to increase, passing through another local minimum at $T_{min2} = 215$ K—see figure 11(b). At $T_{min1} = 260$ K, the integral intensity of the narrow PM line is about 30% of the total EMR spectrum intensity (DIN). Below $T_{p1} = 235$ K on the low-field shoulder of the Lorentzian-like line another strong broad asymmetric line appears and its intensity increases with decreasing temperature. This line shifts toward zero field, having a discontinuity in its resonance field position at $T_{p2} = 180$ K (figure 10(b)). Below $T_{p3} = 125$ K the weak narrow line disappears (see, for instance, the EMR spectrum at $T = 122$ K in figure 8(b)).

4. Discussion

In the following we will discuss the experimental observations described above. A very small variation in the lattice constants was found in the self-doped samples in comparison to those

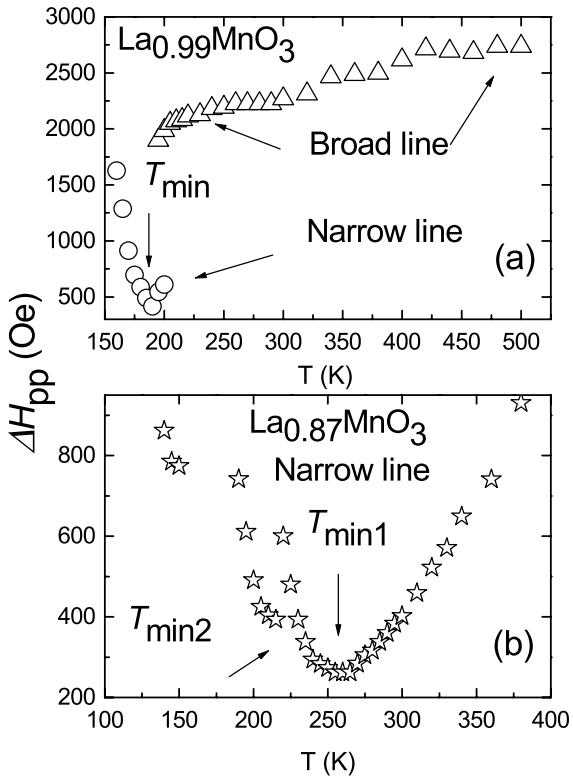

Figure 11. Temperature dependences of the linewidth: (a) $La_{0.99}MnO_3$: circles—narrow PM line; triangles—broad PM line; (b) $La_{0.87}MnO_3$: stars—narrow line; two minima are clearly seen.

of $LaMnO_3$. This allows us to suppose that the magnetic and orbital orders of the samples studied are similar to those of $LaMnO_3$. The increase of the FM moment M_0 with self-doping (see figure 3(b)) may be attributed to the coexistence of an AFM phase and FM clusters at low temperature [6, 8]. The following scenario was proposed by Topfer and Goodenough [6]. Small-polaron holes become increasingly trapped at cation vacancies when the temperature decreases. In orthorhombic structures these trapped holes form superparamagnetic clusters with short-range FM order that become magnetically coupled with the onset of AFM order to constitute a magnetic glass [6]. A similar model was also considered in [8, 10]. It was supposed that the self-doped system is separated into two phases at low temperatures, namely a hole-free AFM insulating phase and hole-rich FM regions with optimal hole concentration $x = 0.25$–0.3 [8]. The two phases are coupled through SE at their interface. As a result of this interaction, the FM cluster cants the surrounding spins in the AFM matrix leading to weakening of the AFM interactions in hole-free phase [8]. In such a case the FM clusters may exhibit a high enough Curie temperature, higher than T_N for the AFM matrix, and the decrease of the pressure coefficient of T_N may reflect some kind of competition between AFM SE interactions in the matrix and FM DE inside the FM clusters. In the case of $La_{0.99}MnO_3$ the amount of FM phase is relatively small, and the pressure coefficient of T_N is close to that of $LaMnO_3$; see figure 4(b). As self-doping increases, the volume of FM clusters increases as well. Then, with increasing volume of FM clusters, an increase of the AFM interaction in the matrix under pressure may be partly counterbalanced by a bigger increase of the DE interaction in FM clusters and, as a result, the pressure coefficient of T_N decreases with self-doping.

There was support for the notion that very low-doped manganites have a canted magnetic structure [2, 4, 7, 8]. An alternative approach explains the experimental MR data at low doping in terms of coexisting of AFM and FM phases where the AFM phase could be a canted one [1]. All self-doped samples studied exhibit practically the same temperatures of magnetic ordering and similar dependences of the magnetization on H and T. This is some indication that their magnetic structures and magnetic anisotropies are similar to those of pure $LaMnO_3$. In principle, we do not rule out a difference between the crystallographic structures of AFM and FM regions, though our x-ray measurements do not show any indication of that within the accuracy of the data analysis (∼1–2%). Magnetization measurements [22] of $LaMnO_3$ crystal show a weak moment of 0.18 μ_B/Mn at $T = 4.2$ K directed along the c-axis, while other measurements revealed the existence of small moments along both the a- and b-axes [25]. In a two-sublattice model, the antisymmetric and anisotropic DM interaction between spins i, j, $E_{DM} = \sum_{i>j} D_{ij}[S_i \times S_j]$, is responsible for the canting of their magnetic moments. The linear dependence of the spontaneous magnetization M_0 versus x (figure 3(b)) allows us to estimate both the spontaneous magnetic moment and the canting angle in $LaMnO_3$. Extrapolating M_0 to $x = 0$, we obtain $M_0 = 2.28$ emu g^{-1}, corresponding to a weak FM moment of 0.09 μ_B. The canting angle obtained is $\alpha = M_0/2M_s \approx 0.7°$. This value is less than the value obtained from measurements of magnetization [22] (∼1°) and implanted muons [26] (∼2°) in pure $LaMnO_3$ crystal. It should be noted that the value of α obtained in all the above measurements might be overestimated due to effects of off-stoichiometry in $LaMnO_3$.

The absence of the MR effect in $La_{0.99}MnO_3$ single crystal may be a result of the very small volume fraction of FM clusters in the AF matrix. Figure 6(a) shows a set of normalized resistivity curves $\rho(H)/\rho(H = 0)$ for $La_{0.87}MnO_3$ crystal at different temperatures. One sees that the largest effect of MR appears at temperatures higher than transition temperature, most probably due to a contribution from FM clusters near La vacancies at $T \sim 200$–220 K. The eight Mn ions surrounding a La vacancy are crystallographically and electronically equivalent and this leads to the creation of neighbouring Mn^{3+}–Mn^{4+} pairs [8] ferromagnetically coupled through strong DE interaction. The above scenario is supported by the temperature dependence of the resistivity, which changes from a semiconducting-like one in the interval $240 < T < 295$ K to a weakly temperature-dependent resistivity at $180 < T < 210$ K; see figure 5. With temperature decreasing below T_N, the MR effect becomes more similar to that of FM polycrystalline samples, which exhibit a sharp resistivity drop at low magnetic fields [1]. Such a similarity may stem from a partial resemblance of transport mechanisms. The low-field MR effect, observed in polycrystalline ceramics of doped manganites, may be attributed to spin-dependent transport between two grains having almost fully polarized charge carriers and the alignment of their magnetization by an applied field [1]. An electronic current in self-doped $La_{0.87}MnO_3$ crystal may be significantly affected by spin-dependent tunnelling between FM clusters. In contrast to the expected quadratic dependence of the MR on magnetic field for phase-separated (PS) manganites [27], a rather linear MR effect versus H is observed for $La_{0.87}MnO_3$ crystal (figure 6(a)). Moreover, the MR effect for $La_{0.87}MnO_3$ crystal at $100 < T < 200$ K depends very slightly on temperature, whereas according to [27] the MR should decrease with temperature as T^{-n}, where n varies from 2 up to 5, depending on the manganite system.

The non-ohmic effects reflect the nature of the interaction between electric current/field and local magnetic moments. For $La_{0.99}MnO_3$ a relatively small increase of the differential resistivity R_d at $T = 200$ K was observed. At room temperature no visible change in R_d is seen. Previous measurements [18, 19] of R_d versus applied current have shown that current flowing across the crystal leads to a decrease in the resistivity and therefore the observed opposite effect

in $La_{0.99}MnO_3$ is quite unexpected. Similar to current effects in hole-doped $La_{0.82}Ca_{0.18}MnO_3$ crystal [19], a weak decrease in R_d with current was observed in $La_{0.87}MnO_3$ even at room temperature (see figure 6(b)). The observed bell-shaped form of the $R_d(I)$ dependences here may also be attributed to spin-polarized tunnel conduction, which modifies the PS configuration and percolation path [19]. An electric field may also induce a local electrical moment in MnO_6 octahedra by modifying the spatial distribution of their charges and the suppression of the JT local distortion.

The results of the EMR measurements carried out on $La_{0.99}MnO_3$ and $La_{087}MnO_3$ samples give direct and unambiguous evidence of a complicated PS state in these self-doped manganites. As clearly seen from the EMR, both compounds exhibit inhomogeneous magnetic phases at low temperatures. However, the precursors of such inhomogeneous magnetic states may be easily observed in the high-temperature PM region. Two PM subsystems were found. The first one is represented by a narrow Lorentzian-like signal with $g = 1.97$, which arises for all Mn^{3+}–Mn^{4+} ions coupled by DE [28]. This signal has the characteristic linewidth dependence: it passes through a minimum and increases upon raising T [29, 30]. Such a subsystem is a common precursor of FM ordered phases in doped manganites (see, for instance, [21, 28]). A broad line, characterizing by $\Delta H_{pp} \sim 2200$ Oe at 300 K, $g = 1.91$, and the weak temperature dependence of the linewidth—see figure 11(a)—represents a second subsystem. An analogous broad line ($\Delta H_{pp} \sim 2500$ Oe at room temperature) was observed in pure $LaMnO_3$ and ascribed to Mn^{3+} ions within an intermediate octahedral ligand field with a tetragonal JT distortion [31, 32]. Hence, we may suppose that the broad line, observed for the two La-deficient samples, arises from Mn^{3+} ions. The g-value observed ($g < 2$) and weak temperature dependence of the broad line width just strengthen the support for this supposition.

At low T, both PM subsystems evolve towards ordering, which is responsible for the more complicated magnetic state. Therefore, the broad line for the $La_{0.99}MnO_3$ sample disappears exactly below $T = 140$ K which coincides well with the Néel temperature of this compound ($T_N \sim 139$ K). It may be supposed that for $La_{0.99}MnO_3$, most of the Mn^{3+} subsystem (about 90%, as was determined by integration) remains unperturbed and accounts for the AFM phase of this compound. On the other hand, the La vacancies create domains of Mn^{4+} ions coupled to the surrounding Mn^{3+} ions by DE. The latter Mn^{3+}–Mn^{4+} subsystem might be responsible for the FM phases observed. The same scenario could be used for $La_{0.87}MnO_3$. However, as was noted previously, here the total weight of the exchange-coupled Mn^{3+}–Mn^{4+} subsystem is about three times higher than that for $La_{0.99}MnO_3$. This may lead to enhancement of the spontaneous magnetization of $La_{0.87}MnO_3$ compared to that for $La_{0.99}MnO_3$ (figure 3(b)).

The magnetically ordered state for both La-deficient compositions was found to be inhomogeneous and to possess AFM and FM phases. The coexistence of these phases may be responsible for the sharp drop of the EMR signal intensities from FM phases below T_{max} (figure 9). We observed this effect earlier for several PS manganites [21] and described it using a FM cluster glass (CG) model. It should also be noted that both samples show quite complicated FMR signals. Two of the three EMR lines observed in spectra of $La_{0.99}MnO_3$, which diverge towards high and low fields, could be interpreted as signals from an anisotropic FMI phase [21]. The third FMR line, shifting towards zero field, is typical for FMM phases. It is worth mentioning that the intensities of the signals from these two magnetic phases are approximately the same. Another kind of magnetic inhomogeneity is observed in the $La_{0.87}MnO_3$ sample. Here at least two typical FMM signals, appearing at $T_{p1} = 235$ K and $T_{p2} = 180$ K are easily distinguished. In particular, just the transformations of these EMR signals on crossing the aforementioned transition points lead to a discontinuity in the temperature dependence of the resonance field (figure 10(b)), as well as to the appearance of the double minima in the temperature dependence of the linewidth (figure 11(b)). Down to

125 K these FMM phases coexist with the PM phase, which also orders magnetically below $T_{p3} = 125$ K. The reason for such a variety of FM phases lies, presumably, in the strong inhomogeneity of the La vacancy distribution. Thus, domains with higher concentrations of Mn^{4+} are responsible for higher transition temperatures. It is worth mentioning here that the above-noted inhomogeneity in $La_{0.87}MnO_3$ may arise due to the exceeding of the limiting concentration for uniform accommodation of La vacancies in the $La_{1-x}MnO_3$ structure [11].

In summary, experiments involving measurements of the magnetization under pressure and resistivity versus temperature, current, and magnetic field, as well as EMR, were employed in our studies of magnetic and transport properties of $La_{1-x}MnO_3$ ($x = 0.01, 0.05, 0.11, 0.13$) single crystals. The results obtained provide further substantiation for the assertion of the existence of mixed magnetic phases at low temperatures, namely an AFM insulating phase and FMM clusters. Although the AFM ordering temperatures for all samples are practically the same, $T_N = 138$–139 K, the spontaneous magnetization and coercive field exhibit a linear increase with x. To the best of our knowledge this is the first time that the dependence of the pressure coefficient $\mathrm{d}T_N/\mathrm{d}P$ has been systematically measured for self-doped manganites. It is supposed that the observed diminution of the pressure coefficient $\mathrm{d}T_N/\mathrm{d}P$ with increasing self-doping stems from the competition of DE operating in FM clusters and AFM SE in the matrix. A clear indication of a PS state in the $La_{1-x}MnO_3$ crystals under consideration was obtained using resistivity measurements. It is found that FM clusters exist in the PM phase above T_N. The relatively large negative MR observed in $La_{0.87}MnO_3$ crystal above T_N may be governed by DE operating within such FM clusters. The dependence on current of the resistivity in $La_{0.87}MnO_3$ single crystal may be attributed to spin-polarized tunnelling conduction, which modifies the local phase separation along the percolation path. The temperature-dependent EMR measurements on $La_{0.99}MnO_3$ and $La_{0.87}MnO_3$ crystals also directly evidenced that the magnetic ordering in these samples is an inhomogeneous one, comprising AFM and various FM phases. For the first time, nearly non-interacting Mn^{3+} and Mn^{3+}–Mn^{4+} subsystems were found in the PM region. They are supposed to be responsible for the AFM and FM phases existing at lower temperatures. It is found that the change of the La vacancy concentration from 0.01 to 0.13 in these crystals increases the volume of the DE-coupled Mn^{3+}–Mn^{4+} subsystem by a factor of 3. This effect, in turn, causes the rise in the total amount of FM phase detected by means of EMR and accounts for the increase of the spontaneous magnetization.

Acknowledgments

This research was supported by the Israeli Science Foundation administered by the Israel Academy of Sciences and Humanities (grant 209/01). Additional support was given by the European Community (programme ICA1-CT-2000-70018, Centre of Excellence CELDIS).

References

[1] Coey J M D, Viret M and von Molnar S 1999 *Adv. Phys.* **48** 167
Dagotto E, Hotta T and Moreo A 2001 *Phys. Rep.* **344** 1
[2] Matsumoto G 1970 *J. Phys. Soc. Japan* **29** 606
[3] Rodriguez-Carvajal J, Hennion M, Moussa F, Moudden A H, Pinsard L and Revcolevschi A 1998 *Phys. Rev.* B **57** R3189
[4] Millis A J, Littlewood P B and Shraiman B I 1995 *Phys. Rev. Lett.* **74** 5144
[5] van Roosmalen J A M, Cordfunke E H P, Helmholdt R B and Zandbergen H W 1994 *J. Solid State Chem.* **110** 100
van Roosmalen J A M and Cordfunke E H P 1994 *J. Solid State Chem.* **110** 106
[6] Topfer J and Goodenough J B 1997 *J. Solid State Chem.* **130** 117
Topfer J and Goodenough J B 1997 *Chem. Mater.* **9** 1467

[7] Prado F, Sanchez R D, Caneiro A, Causa M T and Tovar M 1999 *J. Solid State Chem.* **146** 418
[8] Muroi M and Street R 1999 *Aust. J. Phys.* **52** 205
[9] de Brion S, Ciorcas F, Chouteau G, Lejay P, Radaelli P and Chaillout C 1999 *Phys. Rev.* B **59** 1304
[10] Loshkareva N N, Sukhorukov Yu P, Neifel'd E A, Arkhipov V E, Korolev A V, Gaviko V S, Panfilova E V, Dyakina V P, Mukovskii Ya M and Shulyatev D A 2000 *JETP* **90** 389
[11] Joy P A, Sankar C R and Date S K 2002 *J. Phys.: Condens. Matter* **14** L663
[12] Gupta A, McGuire T M, Duncombe P R, Rupp M, Sun J Z, Gallagher W J and Xiao Gang 1995 *Appl. Phys. Lett.* **67** 3494
[13] Markovich V, Rozenberg E, Gorodetsky G, Revzin B, Pelleg J and Felner I 2000 *Phys. Rev.* B **62** 14186
[14] Markovich V, Rozenberg E, Gorodetsky G, Greenblatt M and McCarroll W H 2001 *Phys. Rev.* B **63** 054423
[15] Pinsard-Gaudart L, Rodriguez-Carvajal J, Daoud-Aladine A, Goncharenko I, Medarde M, Smith R I and Revcolevschi A 2001 *Phys. Rev.* B **64** 064426
[16] Loa I, Adler P, Grzechnik A, Syassen K, Schwarz U, Hanfland M, Rozenberg G Kh, Gorodetsky P and Pasternak M P 2001 *Phys. Rev. Lett.* **87** 125501
[17] Zhou J S and Goodenough J B 2002 *Phys. Rev. Lett.* **89** 087201
[18] Asamitsu A, Tomioka Y, Kuwahara H and Tokura Y 1997 *Nature* **388** 50
[19] Yuzhelevski Y, Markovich V, Dikovsky V, Rozenberg E, Gorodetsky G, Jung G, Shulyatev D A and Mukovskii Ya M 2001 *Phys. Rev.* B **64** 224428
[20] Shulyatev D A, Arsenov A A, Karabashev S G and Mukovskii Ya M 1999 *J. Cryst. Growth* **198/199** 511
[21] Markovich V, Rozenberg E, Shames A I, Gorodetsky G, Fita I, Suzuki K, Puzniak R, Shulyatev D and Mukovskii Ya M 2002 *Phys. Rev.* B **65** 144402
[22] Skumryev V, Ott F, Coye J M D, Anane A, Renard J P, Pinsard-Gaudart L and Revcolevschi A 1999 *Eur. Phys. J.* B **11** 401
[23] Maurin I, Barboux P, Lassailly Y, Boilot J P, Villain F and Dordor P J 2001 *Solid State Chem.* **160** 123
[24] Loshkareva N N, Korolev A V, Arbusova T I, Solin N I, Viglin N A, Smolyak I B, Bebenin N G, Sukhorukov Yu P, Naumov S V, Kostromitina N V and Balbashov A M 2002 *Phys. Solid State* **44** 1916
[25] Mitsudo S, Hirano K, Nojiri H, Motokawa M, Hirota K, Nishizawa A, Kaneko N and Endoh Y 1998 *J. Magn. Magn. Mater.* **177–181** 877
[26] Guidi M C, Allodi G, De Renzi R, Guidi G, Hennion M, Pinsard L and Amato A 2001 *Phys. Rev.* B **64** 064414
[27] Sboychakov A O, Rakhmanov A L, Kugel K I, Kagan M Yu and Brodsky I V 2002 *JETP* **95** 753
[28] Causa M, Tovar M, Caneiro A, Prado F, Ibanez G, Ramos C, Butera A, Alascio B, Obradors X, Pinol S, Rivadulla F, Vazquez-Vazquez C, Lopez-Quintela M, Rivas J, Tokura Y and Oseroff S B 1998 *Phys. Rev.* B **58** 3233
[29] Huber D L, Alejandro G, Caneiro A, Causa M T, Prado F, Tovar M and Oseroff S B 1999 *Phys. Rev.* B **60** 12155
[30] Shengelaya A, Zhao Guo-meng, Keller H, Müller K A and Kochelaev B I 2000 *Phys. Rev.* B **61** 5888
[31] Granado E, Moreno N O, Garcia A, Sanjurjo J A, Rettori C, Torriani I, Oseroff S B, Neumeier J J, McClellan K J, Cheong S W and Tokura Y 1998 *Phys. Rev.* B **58** 11435
[32] Eremin V A, Deisenhofer J, Krug von Nidda H A, Loidl A, Mukhin A A, Balbashov A M and Eremin M V 2000 *Phys. Rev.* B **61** 6213